Tailoring the vortex pinning strength of YBCO thin films by systematic incorporation of hybrid artificial pinning centers

Tailoring the vortex pinning strength of YBCO thin films by systematic incorporation of hybrid artificial pinning centers

Alok K. Jha[1]*, Kaname Matsumoto[1], Tomoya Horide[1], Shrikant Saini[2†], Paolo Mele[3], Ataru Ichinose[4], Yutaka Yoshida[5], Satoshi Awaji[6]

[1] *Department of Materials Science and Engineering, Kyushu Institute of Technology, Tobata-ku, Kitakyushu 804-8550, Japan*

[2] *Institute for Sustainable Sciences and Development, Hiroshima University, 739-8530 Higashi-Hiroshima, Japan*

[3] *Materials Science Research Unit, Muroran Institute of Technology, 050-8585 Mizumoto-cho, Muroran, Japan*

[4] *Central Research Institute of Electrical Power Industry, Yokosuka, Kanagawa 240-0196, Japan*

[5] *Department of Energy Engineering and Science, Nagoya University, Chikusa-ku, Nagoya 464-8603, Japan*

[6] *Institute for Materials Research, Tohoku University, Aoba-ku, Sendai 980-8577, Japan*

* E-mail: akjha@post.matsc.kyutech.ac.jp

† *Present address: Department of Materials Science and Engineering, University of Utah, Salt Lake City, UT 84112, USA*

Abstract

The effect of hybrid (columnar and spherical together) artificial pinning centers (APCs) on the vortex pinning properties of YBCO thin films is investigated in detail on the basis of variation of critical current density (J_C) with applied magnetic field and also with the orientation of the applied magnetic field at 65 K and 77 K. Premixed YBCO+BaSnO$_3$ composite targets are used for the deposition of the YBCO films consisting of self-assembled BaSnO$_3$ nanocolumns (1-D APCs) whereas for the deposition of the YBCO films with hybrid APCs (BaSnO$_3$ nanocolumns together with Y$_2$O$_3$ nanoparticles), the surface of the premixed YBCO+ BaSnO$_3$ composite targets are

modified by putting a thin Y_2O_3 sectored piece on the premixed target by means of silver paste. $F_{pmax.}$ value increases systematically with incorporation of 1-D and 1-D+3-D APCs and it also shifts towards higher applied magnetic fields. Films with 1-D APCs exhibits strong J_C peak at $\Theta = 0°$ (H//c-axis) whereas films consisting of hybrid APCs exhibit enhanced J_C at all the investigated angular regime. A possible mechanism of vortex pinning in samples with hybrid APCs is also discussed suggesting the role of 1-D and 3-D APCs.

1. Introduction

$YBa_2Cu_3O_{7-\delta}$ (YBCO) thin films with high supercurrent carrying capability and low anisotropy over wide range of temperature and applied magnetic field are strongly desired for various technological applications [1-3]. The enhancement of critical current density (J_C) and the reduction of the anisotropy in the J_C has been the subject of intense activity in recent years. In YBCO thin films, there is vortex pinning due to the presence of naturally occurring defects such as dislocations, oxygen vacancies, grain boundaries, twin boundaries, etc. However, majority of these defects are unable to prevent the vortex motion due to thermal fluctuations which is needed to maintain the necessary level of critical current density at large magnetic fields [4-5]. The introduction of artificial pinning centers (APCs) into YBCO superconducting film matrix has been recognized as being very effective for the immobilization of vortices leading to enhanced critical current density (J_C) of YBCO films. Various methodologies have been employed to introduce APCs into YBCO films which include irradiating the film with

heavy ions [6], addition and/or substitution of rare-earth atoms [7, 8] or by adding the secondary phase nanoinclusions into the YBCO film matrix [9-18]. The incorporation of secondary phase nanoinclusions into YBCO superconducting film matrix for improving the vortex pinning properties has recently been extensively studied. The nanoinclusions of several non-perovskite, perovskite and double-perovskite materials such as Y_2BaCuO_5 [9], Y_2O_3 [10], $BaZrO_3$ [11, 12], $BaSnO_3$ [13, 14], $BaIrO_3$ [15], YBa_2NbO_6 [16, 17], YBa_2TaO_6 [18] have been demonstrated to enhance the vortex pinning properties of YBCO films deposited by pulsed laser deposition (PLD) technique. The critical current density of YBCO films exhibit intrinsic anisotropy where at a particular magnetic field; J_C along the *ab*-plane is higher than along the *c*-axis which is attributed to the anisotropic crystal structure of YBCO. The self-assembled nanocolumns of perovskite such as $BaZrO_3$ (BZO), $BaSnO_3$ (BSO), YBa_2NbO_6 (YBNO) etc. have been very effective in improving the J_C particularly when the magnetic field is oriented along the *c*-axis of the films. At elevated temperatures, however, even if the film matrix contains *c*-axis correlated disorders, the vortices may form double kink structures due to thermal excitations and because of this the unpinned vortex segments can move under the influence of Lorentz force. Also, when the applied magnetic field is tilted from the *c*-axis, the correlated disorders start losing the vortices gradually and at enough inclination, vortices become free from the correlated disorders. It is, therefore, highly desirable to incorporate additional or a combination of pinning structures which could provide pinning to vortices even when the applied magnetic field is tilted from the *c*-axis leading to enhanced critical current density in the intermediate angular regime (between *ab*- plane and *c*-axis) as well.

One of the earliest reports on the use of different kinds of pinning centers together in

YBCO thin films was made by Mele *et al.* [19] in which both columnar (BZO) as well as spherical Y_2O_3 (YO) nanostructures were inserted into the YBCO film matrix. They observed slight enhancement in the J_C along the intermediate angular regime but the *c*-axis J_C peak was found to be suppressed. In another report, Maiorov *et al.* [20] have observed the formation of short and splayed columnar nanostructures as result of varying deposition temperature and they found that such short and splayed columnar nanostructures are effective for pinning of vortices even when the magnetic field is tilted from the *c*-axis. The combination of YO nanoparticles and YBNO nanocolumns has been reported by Feldmann *et al.* [16] where the anisotropy of J_C of YBCO film was controlled. In a recent report, Horide *et al.* [21] have shown that the incorporation of hybrid structures (1-D nanocolumns together with 3-D nanoparticles) into YBCO films on metallic tapes reduces the anisotropy at 77 K. In their report, however, anisotropy reduction is observed only for one composition at a particular temperature and applied magnetic field.

In the PLD technique, the secondary phase nanoinclusions are usually introduced into the YBCO matrix by two methods: one by premixing the secondary phase material with YBCO and making a mixed target. Another approach is to use two different targets of YBCO and secondary phase material and switching them alternatively and periodically during deposition. A novel approach for introducing nanoscale secondary phase inclusions in YBCO film using pulsed laser deposition technique is to use surface modified target in which a thin sectored piece of secondary phase material is attached on the top of YBCO target using silver paste [19, 22]. There are several advantages of this approach over others, one of which is that the APCs can be continuously introduced into YBCO film matrix using single target in which YBCO portion and secondary phase

4

material portion are physically separate. Another advantage of this approach is that the content of the secondary phase material can be finely tuned by changing the size of the sectored piece of secondary phase material while keeping the YBCO target as the same. In this paper, detailed investigation on the effect of BSO and YO hybrid nanostructures on the vortex pinning properties of YBCO thin films is presented. For incorporating BSO nanocolumns, premixed YBCO+BSO targets are used whereas for incorporating YO nanoparticles, thin sectored YO pieces are attached on top of the premixed YBCO+BSO composite target surface. The concentrations of secondary phase nanoinclusions are controlled by changing the concentration of BSO in the premixed targets (2%, 3% and 4% by weight) and varying the area of the YO sectored pieces (2.2% of target area and 3% of target area). The nanocomposite thin films comprising of hybrid APCs showed superior J_C-B characteristics along with significantly improved angular dependence both at 77 K as well as 65 K. In addition, the irreversibility field is calculated for all the samples and its variation with temperature is studied as well. The role of hybrid APCs in the shifting the irreversibility line towards higher B-T regime is also discussed.

2. Experimental details

Pristine YBCO film and YBCO films consisting of BSO and BSO+YO hybrid APCs have been deposited on single crystal SrTiO$_3$ (STO) substrates using PLD technique (KrF excimer laser, λ = 248 nm). The schematic diagram of the deposition chamber is shown in figure 1 (a). The substrate temperature of 830℃ and O$_2$ partial pressure of 0.26 mbar was maintained during the deposition of the films. A repetition rate of 10 Hz was used while substrate to target distance was kept as 60 mm. For the deposition of YBCO thin film, a pristine YBCO target was used and for YBCO+BSO nanocomposite

films, pre-mixed YBCO+BSO targets were used. For YBCO+BSO+YO films the surface of the same pre-mixed YBCO+BSO target is modified as schematically illustrated in figure 1 (b). The concentration BSO nanocolumns in the samples is varied by varying the BSO concentration in the pre-mixed target as 2%, 3% and 4% (by weight) and the concentration of YO nanoparticles is varied by modifying the target surface with two different sizes of sectored yttria pieces: 2.2 area % and 3 area % which are referred as YOA and YOB in this paper onwards. As the target is rotated, the YO portion is periodically ablated allowing the formation of YO nanoparticles together with BSO nanocolumns in the YBCO film matrix.

The structural characterization of the pristine YBCO and YBCO films with APCs was done using X-ray diffractometer (Bruker D8 XRD) with Cu-Kα radiation. The Θ-2Θ diffraction data were collected over diffraction angles ranging from 2Θ = 10°–80°. ω-scan and ϕ-scan were also carried out to observe the in-plane and out-of plane symmetries. The cross-sectional microstructure of YBCO+BSO and YBCO+BSO+YO nanocomposite films have been studied using transmission electron microscope (TEM: H-9000NAR, Hitachi Co. Ltd.). The high resolution TEM images are taken by JEOL JEM-2100F.

Microbridges of 1 mm length and 60 μm width have been fabricated on the thin film samples using photolithography and wet-chemical etching technique for critical current measurements. Transport properties of these thin film samples have been measured using four-probe method by a Physical Property Measurement System (PPMS, Quantum Design). A voltage criterion of 1 μVcm^{-1} has been used to obtain the critical current values. Angular dependence of J_C of all the thin film samples was measured at 77 K, 1 T and 65 K, 3 T using the same voltage criterion. Resistivity versus temperature

6

measurements were carried out at difference applied magnetic fields to determine the irreversibility lines for all the samples.

3. Results and discussion

The strong c-axis orientation of pristine YBCO, YBCO+BSO and YBCO+BSO+YO nanocomposite films has been ascertained from the X-ray diffraction measurement. The in-plane orientation has also been found to be reasonably good for all the thin film samples. The c-axis for the YBCO films with APCs, however, exhibited relative expansion compared to the pristine YBCO film. The structural parameters as obtained from X-ray diffraction measurement for all the thin film samples are listed in table 1. The $\Delta\omega$ of YBCO(005) peak for all the samples vary between 0.14° and 0.27° except for YBCO+BSO2%+YOA sample for which it is relatively higher (0.46). $\Delta\phi$ of YBCO(103) is measured for all samples vary between 1.05° to 1.38° indicating that out of plane symmetries for the samples are also reasonably good. In figure 2, the typical cross-sectional transmission electron micrographs of (a) YBCO+BSO2%, (b) YBCO+BSO2%+YOB, (c) YBCO+BSO4%, and (d) YBCO+BSO4%+YOB nanocomposite films are shown. In all the TEM images, the formation of nanocolumnar structures can be observed clearly. In YBCO+BSO+YO films, however, the formation of nanoparticles can also be observed which are supposed be of YO. The self-assembled BSO nanocolumns are oriented along the c-axis of the films. From the TEM images of the samples [figure 2(a) and (c)], the density of BSO nanocolumns can be estimated for YBCO+BSO2% and YBCO+BSO4% films by extrapolating the linear density into the areal density. Such an estimation leads us to obtain the BSO nanocolumn density of 4.1 $\times$ 10^{11} cm^{-2} and 5.7 $\times$ 10^{11} cm^{-2} in YBCO+BSO2% and YBCO+BSO4% films respectively. However, such an estimation has the possibility of some errors as the

density of defects may vary along different directions. Moreover, it is difficult to estimate the density of Y_2O_3 nanoparticles in the hybrid APC samples because these are not so distinctly visible in these images. In figure 3, the cross-sectional TEM image at higher magnification for (a) YBCO+BSO2%+YOA and (b) YBCO+BSO4%+YOA films are shown. In the cross-sectional image of YBCO+BSO2%+YOA sample, apart from the c-axis oriented nanocolumns, some planar defects are also observed which might be stacking faults originated during the growth of the film or may be due to associated BSO/YO nanostructures in the vicinity. Also shown in the insets are the planar views of the TEM image of the respective samples. From the planar view, it can be observed that the BSO nanocolumns are uniformly distributed in the YBCO matrix. From the planar view of the TEM image, a rough estimation of the matching field is made which comes out to be ~2.5-3.5 T.

The critical temperatures (T_C) of all the superconducting thin film samples are obtained from electrical transport measurement. The T_C for pristine YBCO film is 89.8 K. The T_C values for YBCO+BSO2%, YBCO+BSO2%+YOA and YBCO+BSO2%+YOB films are 89.7 K, 86.7 K and 89.7 K respectively. For YBCO+BSO3%, YBCO+BSO3%+YOA and YBCO+BSO3%+YOB thin film samples, the T_C values are 86.6 K, 89.3 K and 88.7 K respectively and YBCO+BSO4%, YBCO+BSO4%+YOA and YBCO+BSO4%+YOB thin film samples have their T_C values as 89.2 K, 89.1 K and 88.4 K respectively. The T_C of all the samples is more than 88 K except for YBCO+BSO2%+YOA and YBCO+BSO3% samples for which it is relatively lower. The interfacial strain in the YBCO film has been studied by Zhai *et al.* [23] and they found that it is one of the factors for the reduction of T_C in YBCO films. However, as the strain is relieved by dislocations and other growth defects, this reduction is not

observed. In the high resolution TEM image of YBCO+BSO2%+YOA film, lot of planar defects have been observed and which could lead to increased $\Delta\omega$ of the film this also could be another reason for the reduction of the T_C in this film.

Irreversibility field ($B_{irr.}$) is an important superconducting parameter which determines the magnetic field above which dissipation free transport current ceases and the prospect of technological applications rely upon improved $B_{irr.}$ of YBCO films by means of APCs. Resistivity versus temperature measurements were performed in different magnetic fields from 0 to 9 T to obtain the irreversibility lines of all the samples. Incorporating APCs shifts the irreversibility lines towards higher temperature regime at lower field and a shoulder is formed in the irreversibility line. This up-shift of the irreversibility line is explained by the formation of a Bose glass, i.e. by pinning at correlated columnar defects up to a matching field as predicted by Nelson and Vinokur [24]. The intersection of the curved portion and the straight line portion of the irreversibility line is used to estimate the matching field of the superconducting sample. In figure 4, the variation of $B_{irr.}$ with respect to temperature is presented for (a) YBCO+BSO2% series, (b) YBCO+BSO3% series, (c) YBCO+BSO3% series and (d) all samples together. According to the figure, the matching fields of the samples vary between ~2-4 T and it is consistent with what is estimated from the planar view of the TEM image. In cases, when the irreversibility line does not cross 77 K till 9 T, $B_{irr.}$ at 77 K is determined by extrapolating the straight line portions of the irreversibility lines. For YBCO film, $B_{irr.}$ at 77 K is obtained as 7.8 T whereas for YBCO+BSO2%, YBCO+BSO2%+YOA and YBCO+BSO2%+YOB, it is obtained as 10.1, 9.5 and 8.3 T respectively. In this series of samples, by incorporating the YO nanoparticles and increasing their concentration, $B_{irr.}$ is found to decrease. In the case of BSO3% series samples, $B_{irr.}$ for YBCO+BSO3%,

9

YBCO+BSO3%+YOA and YBCO+BSO3%+YOB films is obtained as 10.4, 11.3 and 10.8 T respectively whereas in the case of BSO4% series samples, $B_{irr.}$ for YBCO+BSO4%, YBCO+BSO4%+YOA and YBCO+BSO4%+YOB films is obtained as 11.8, 11 and 11.6 T respectively. There is no systematic pattern in the variation of $B_{irr.}$ values of the samples with respect to YO concentration. It can be said that incorporating YO nanoparticles does not have any significant effect on $B_{irr.}$ of YBCO films.

In figure 5, the variation of J_C and F_p (pinning force density) with respect to applied magnetic field for YBCO, YBCO+BSO (single APC) and YBCO+BSO+YO (hybrid APCs) nanocomposite films has been presented at 77 K (a), (b) and 65 K (c), (d). It can be observed that at applied magnetic fields, the J_C values of the YBCO films with APCs are increased significantly. In both YBCO+BSO2% series and YBCO+BSO3% series samples, as the YO nanoparticles are incorporated and their concentration are increased, the J_C-B characteristics get improved. However, in the case of YBCO+BSO4% series samples, the incorporation of YO leads to the degradation of the J_C-B characteristics as compared to the J_C-B characteristics of YBCO+BSO4% (single APC) samples. The evidence of improved J_C-B characteristics can be observed in the variation of F_p with applied magnetic field (figure 5(b) and (d)) plots. At 77 K, $F_{pmax.}$ for YBCO film is 2.86 GN.m^{-3} whereas it increases to 5.38, 7.87 and 9.52 GN.m^{-3} for YBCO+BSO2%, YBCO+BSO2%+YOA and YBCO+BSO2%+YOB films respectively. For YBCO+BSO3%, YBCO+BSO3%+YOA and YBCO+BSO3%+YOB films, the $F_{pmax.}$ values are obtained as 8.25, 8.64, 10.91 GN.m^{-3} respectively. There is significant increase in the $F_{pmax.}$ values of the films consisting of 1-D and 1-D+3-D (hybrid) APCs indicating the effectiveness of both BSO nanocolumns and YO nanoparticles as strong pinning centers. Apart from the enhanced $F_{pmax.}$ values, $B_{max.}$ (the applied magnetic field

10

at which $F_{pmax.}$ occurs) is also shifted towards higher values for YBCO films consisting of hybrid APCs, which means that pinning is more effective at higher applied magnetic field in films consisting of hybrid APCs. The $B_{max.}$ values for YBCO+BSO2%, YBCO+BSO2%+YOA and YBCO+BSO2%+YOB samples are 2.2, 2.6 and 4 T respectively and for YBCO+BSO3%, YBCO+BSO3%+YOA and YBCO+BSO3%+YOB films, it is 2, 2.6, 2.8 T respectively. However, in the case of YBCO+BSO4% series samples the scenario is different. For YBCO+BSO4%, YBCO+BSO4%+YOA and YBCO+BSO4%+YOB films, the $F_{pmax.}$ values are obtained as 20.06, 15.89, 10.32 GN.m^{-3} respectively and the $B_{max.}$ values are obtained as 2.2, 2.8 and 2.6 T respectively. For YBCO+BSO4%+YOA sample, although the $F_{pmax.}$ value is decreased as compared to that for YBCO+BSO4% sample, $B_{max.}$ value is higher. For YBCO+BSO4%+YOB sample, however, both $F_{pmax.}$ and $B_{max.}$ values decrease. It can be concluded that the BSO nanorods and YO nanoparticles both are effective to improve the critical current properties of YBCO films if incorporated moderately as observed in YBCO+BSO2% series and YBCO+BSO3% series samples. Too much incorporation, however, is expected to degrade the YBCO superconducting matrix leading to reduction in J_C values as observed in YBCO+BSO4% series samples. In the case of YBCO films incorporating APCs in much higher concentration, the T_C, J_C and the upper critical field become lower in the regions having high concentration of APCs as the superconducting coherence length elongates in comparison with that of the superconducting region having less density of APCs. The weakening of the pinning strength in this region may be attributed to the depressed condensation energy associated with the vortices momentarily displaced by the Lorentz force. The suppressed superconducting parameters may be the result of disappearance of superconductivity in the regions

having much high density of APCs.

At 65 K, $F_{pmax.}$ for YBCO film is 13.6 GN.m^{-3} whereas it increases to 36.08, 45.73, and 57.2 GN.m^{-3} for YBCO+BSO2%, YBCO+BSO2%+YOA and YBCO+BSO2%+YOB films respectively. Similarly, for YBCO+BSO3%, YBCO+BSO3%+YOA and YBCO+BSO3%+YOB films, the obtained $F_{pmax.}$ values are 43.38, 52.80, and 60.13 GN.m^{-3} respectively. In both YCBO+BSO2% and YBCO+BSO3% series samples, the incorporation of hybrid APCs into YBCO films not only increases $F_{pmax.}$ values but also shifts the $B_{max.}$ values towards higher magnetic fields as observed at 77 K. Shifting of $B_{max.}$ towards higher applied magnetic field can be understood in terms of the vortex densities in the hybrid APC samples. When the magnetic field is applied, the flux lines are occupied by the BSO nanocolumns (correlated disorder along the c-axis) till the applied magnetic field is less than or equal to the matching field. However, as the applied magnetic field keeps on increasing, the BSO nanocolumnar structures cannot accommodate any more flux lines around them and here the YO nanoparticles start pinning the flux lines at places between the nanorods. Thus pinning force is provided by both BSO nanocolumns and YO nanoparticles in the samples consisting of the hybrid APCs. Such an explanation seems reasonable for YBCO+BSO2% and YBCO+BSO3% series samples. In the case of YBCO+BSO4% samples, however, the incorporation of YO nanoparticles not only decreases the $F_{pmax.}$ values but also shifts $B_{max.}$ towards lower values on the field axis. Another interesting feature can be observed in the F_p-B characteristics of YBCO+BSO4% sample in which the unusually broad peak is observed which takes place between 2-6 T. Such an unusually broad peak F_p-B plot has also been observed by Feldmann *et al.* [16] at 65 K and also by Xu *et al.* [25] at 4.2 K. Although the exact reason for such a feature is not understood so far, one possible

reason could be the collective pinning of vortices as J_C is inversely proportional to the applied magnetic field.

Figure 6 shows the variation of $F_{pmax.}$ and $B_{max.}$ for YBCO+BSO samples with respect to the YO area percent both at 77 K (a), (b) and at 65 K (c) and (d). It can be observed that for both YBCO+BSO2% and YBCO+BSO3% series samples, $F_{pmax.}$ continues to increase with respect to YO incorporation both at 77 K and at 65 K. In the case of YBCO+BSO4% series however, the incorporation of YO nanoparticles in the given amount leads to the degradation of the $F_{pmax.}$ values at both temperatures. However, if the YO area percent is finely tuned with YBCO+BSO4% films, the effect of YO nanoparticles in improving the $F_{pmax.}$ values are expected to be observed.

In figure 7, the angular variation of J_C for YBCO, YBCO+BSO and YBCO+BSO+YO films measured at 77 K, 1 T is presented. In order to make the appearance distinct, the J_C-B-Θ characteristics for YBCO+BSO2%, YBCO+BSO3% and YBCO+BSO4% series samples have been presented separately along with that of pure YBCO sample in (a), (b) and (c) respectively and finally J_C-B-Θ characteristics for all the samples have been drawn together in (d). Looking at the angular dependent J_C behavior of YBCO+BSO2% series samples (figure 7(a)), it can be observed that all the APC samples exhibit strong J_C peak along the c-axis which is resulted due to c-axis correlated pinning by continuous BSO nanocolumns. However, as the orientation of the magnetic field changes J_C starts decreasing and reaches to minimum before again exhibiting a peak when the applied magnetic field is along the a-b plane. The samples consisting of hybrid APCs (YBCO+BSO2%+YOA and YBCO+BSO2%+YOB), however, exhibit enhanced J_C values in the intermediate angular regime (between a-b plane and c-axis) as well as per the concentration of the YO nanoparticles. In the case of YBCO+BSO3%

13

series samples also, strong J_C peak can be observed for all APC samples and as the YO nanoparticles are added and their concentration is increased, J_C is enhanced in the intermediate angular regime as well. In the case of YBCO+BSO4% series samples, such enhancement of J_C in the intermediate angular regime by YO nanoparticles incorporation is not observed and incorporation of YO nanoparticles reduces J_C values along the entire investigated angular regime.

In figure 8, J_C-B-Θ characteristics for all the samples measured at 65 K, 3 T is presented. Strong improvement in the J_C values is observed both along the c-axis as well as in the intermediate angular regime for samples consisting of hybrid APCs. It is noteworthy here that by adding and increasing the YO content, the c-axis peak remain unchanged. It may be understood in terms of BSO nanocolumns density in the samples containing APCs. Even though YO is added and its content is increased, the BSO concentration remains the same in all samples containing APCs. In the pristine YBCO film the strong J_C peak along the ab-plane is observed because of its layered structure where the weak superconducting layers provide stability to the flux lines when these are parallel to the ab-plane [26]. In the YBCO+BSO3% sample, however, even if the c-axis J_C peak is enhanced significantly, J_C peak along ab-plane is suppressed somewhat presumably because of high density of continuous BSO nanorods which may prevent the intrinsic layer pinning [27]. As the content of YO is added and increased in the samples (hybrid APC samples), the J_C peak along the ab-plane also start becoming pronounced and stronger which means that pinning due to YO nanoparticles is compensating the loss of intrinsic pinning in the samples containing hybrid APC. The samples consisting of hybrid APCs exhibit enhanced J_C values for all orientations of applied magnetic field due to cooperative contributions of both 1-D and 3-D APCs. The increase in the J_C

14

values along the *c*-axis is the consequence of strong pinning of vortices by BSO nanocolumns. Furthermore, in the intermediate angular regime, J_C values are enhanced in the YBCO+BSO+YO sample which contains both BSO nanocolumns providing *c*-axis pinning and YO nanoparticles providing isotropic pinning. As the YO nanoparticles are added (YBCO+BSO+YOA), the enhancement is observed for all angular regime and further increasing the YO content (YBCO+BSO+YOB), the enhancement is most prominent especially in the intermediate angular regime indicating the role of YO nanoparticles providing strong isotropic pinning. In the case of YBCO+BSO4% series samples, however, the effect of such enhancement of J_C in the intermediate angular regime by YO nanoparticles incorporation is not observed and incorporation of YO nanoparticles reduces J_C values along the entire investigated angular regime.

The calculation of J_C values has been proposed by Gurevich [28] and other researchers [29, 30] who considered nanoparticles of materials such as Y_2O_3 or Y211 as strong pinning centers which can pin the bent segments of the vortices strongly. According to such a model, the expression of critical current from the depinning of the curved segments, which are held by two consecutive nanoparticles separated by a distance *d* is given by

$$J_C^{max} = \frac{\Phi_0}{4\pi\mu_0\lambda_{ab}\lambda_c d} ln\frac{d}{\xi_c} \qquad \ldots\ldots\ldots (1)$$

where Φ_0 is the flux quantum, μ_0 is the magnetic permeability, λ_{ab} and λ_c are the London penetration depths in the *ab* plane and along the *c*-axis, respectively, and ξ_c is the coherence length along the *c*-axis. According to this equation, the J_C value is proportional to $\frac{1}{d}ln(\frac{d}{\xi_c})$ and for smaller separation between the nanoparticles (higher

the concentration) higher J_C is expected (using the typical value of $d \sim 10$ nm). However, in a recent report, Mele *et al.* [31] showed that too much incorporation of YO nanoparticles in YBCO matrix leads to the degradation of the J_C values and they attributed it to the high concentration of non-superconducting YO particle leading to hindrance of the current transport.

The reduction of J_C with respect to the orientation of the applied magnetic field has been described by Paulius *et al.* [32]. According to their model, when the magnetic field is oriented at an angle with the *c*-axis of the film, a vortex line which is trapped in the columnar defect has three different regions: a trapped portion of the vortex occupied by the columnar defect and two healing regions relatively free from the columnar defect. As the inclination of the magnetic field with respect to *c*-axis increases, the length of the trapped portion of the vortex decreases and subsequently J_C becomes low. At sufficient inclination, no region of the vortex is trapped and J_C becomes minimum. The schematic diagram depicting such a situation is drawn in figure 9(a). In the present case of samples consisting of hybrid APCs, even though the vortices can become free of the BSO nanocolumns in the intermediate angular regime, the YO nanoparticles can pin different portions of the vortices irrespective of the orientation of the applied magnetic field which results in the improved J_C values along all the magnetic field orientations as shown in figure 9(b).   It, therefore, can be concluded that the combination of 1D+3D APCs is very useful in improving the vortex pinning properties of YBCO films which can be observed in terms improvement of J_C values along all the orientations of the applied magnetic field.

16

Conclusions

We have successfully incorporated BSO+YO hybrid APCs into YBCO film matrix in systematic manner and demonstrated that the hybrid APCs improve the vortex pinning properties of YBCO film significantly provided these are incorporated in moderate concentration. For YBCO+BSO2% series and YBCO+BSO3% series samples, the $F_{pmax..}$ values exhibited systematic increase with increasing the density of hybrid APCs and $B_{max}.$ is shifted towards higher magnetic field indicating more effective vortex pinning at higher applied magnetic field at both the temperatures: 77 K and 65 K. The shifting of $B_{max}.$ towards higher applied magnetic field has been attributed to the strong pinning of vortices by YO nanoparticles. For YBCO+BSO4% series samples, although YBCO+BSO4% film exhibited highest $F_{pmax.}$ value both at 77 K and 65 K, but the incorporation of YO nanoparticles further led to the reduction of $F_{pmax.}$ value. The angular dependence of J_C exhibited significant improvement in the YBCO film with hybrid APCs not only along the *c*-axis but also along the entire investigated angular regime. The BSO nanocolumns (1-D APCs) are supposed to pin the vortices when the flux lines are along the *c*-axis whereas, YO nanoparticles (3-D APCs) supposedly pinned the vortices isotropically, resulting in enhanced J_C values along all the orientations of the applied magnetic fields.

Acknowledgements

References:

[1] D. C. Larbalestier, A. Gurevich, D. M. Feldmann and A. Polyanskii, *Nature* (London) 414, 368 (2001)

[2] S. R. Foltyn, L. Civale, J. L. MacManus Driscoll, Q. X. Jia, B. Maiorov, H. Wang, M. Maley 2007 *Nat. Mater.* **6** 631

[3] Matsumoto K and Mele P 2010 *Supercond. Sci. Technol.* **23** 014001

[4] Dam B, Huijbregtse J M, Klaassen F C, Van der Geest R C F, Doornbos G, Rector J H, Testa A M, Freisem S, Martinez J C, Stauble-Pumpin B and Griessen R 1999 *Nature* **399** 439

[5] Huijbregtse J M, Klaassen F C, Szepielow A, Rector J H, Dam B, Griessen R, Kooi B J and de Hosson J T M 2002 *Supercond. Sci. Technol.* **15** 395

[6] Civale L 1997 *Supercond. Sci. Technol.* **10** A11

[7] Wee S H, Goyal A, Martin P M and Heatherly L 2006 *Supercond. Sci. Technol.* **19** 865

[8] Cai C, Holzapfel B, Hanishch J, Fernandez L and Schultz L 2004 *Phys. Rev. B* **69** 104531

[9] Haugan T, Barnes P N, Wheeler R, Meisenkothen F and Sumption M 2004 *Nature* **430** 867

[10] Gapud A A, Kumar D, Viswanathan S K, Cantoni C, Varela M, Abiade J, Pennycook S J and Christen D K 2005 *Supercond. Sci. Technol.* **18** 1502

[11] MacManus Driscoll J L, Foltyn S R, Jia Q X, Wang H, Serquis A, Civale L, Maiorov B, Hawley M E, Maley M P and Peterson D E 2004 *Nat. Mater.* 3 439

[12] Goyal A, Kang S, Leonard K J, Martin P M, Gapud A A, Varela M, Paranthaman M, Ijaduola A O, Specht E D, Thompson J R, Christen D K, Pennycook S J and

List F A 2005 *Supercond. Sci. Technol.* **18** 1533

[13] Mele P, Matsumpto K, Ichinose A, Mukaida M, Yoshida Y, Horii S and Kita R 2008 *Supercond. Sci. Technol.* **21** 125017

[14] Varanasi C V, Burke J, Wang H, Lee J H and Barnes P N 2008 *Appl. Phys. Lett.* **93** 092501

[15] Hanisch J, Cai C, Huhne R, Schultz L and Holzapfel B 2005 *Appl. Phys. Lett.* **86** 122508

[16] Feldmann D M, Holesinger, T G, Maiorov B, Foltyn S R, Coulter J Y and Apodaca I 2010 *Supercond. Sci. Technol.* **23** 095004

[17] Wee S H, Goyal A, Zuev Y L, Cantoni C, Selvamanickam V and Specht E D 2010 *Appl. Phys. Exp.* **3** 023101

[18] Wee S H, Goyal A, Specht E D, Cantoni C, Zuev Y L, Selvamanickam V and Cook S 2010 *Phys. Rev. B* **81** 140503

[19] Mele P, Matsumpto K, Horide T, Ichinose A, Mukaida M, Yoshida Y and Horii S 2007 *Supercond. Sci. Technol.* **20** 616

[20] Maiorov B, Baily S A, Zhou H, Ugurlu, O, Kennison J A, Dowden P C, Holesinger T G, Foltyn S R and Civale L, 2009 *Nat. Mater.* **8** 398

[21] Horide T, Kawamura T, Matsumoto K, Ichinose A, Yoshizumi M, Izumi T and Shiohara Y 2013 *Supercond. Sci. Technol.* **26** 075019

[22] Varanasi C, Barnes P N, Burke J, Carpenter J and Haugan T 2005 *Appl. Phys. Lett.* **87** 262510

[23] Zhai H Y and Chu W K 2000 *Appl. Phys. Lett.* **76** 3469

[24] Nelson D R and Vinokur V M 1992 *Phys. Rev. Lett.* **68** 2398

[25] Xu A, Delgado L, Khatri N., Liu Y, Selvamanickam V, Abraimov D, Jaroszynski J,

Kametani F and Larbalestier D C 2014 *APL Mater.* **2** 046111

[26] Tachiki M and Takahashi S 1989 *Sol. St. Comm.* **72** 1083

[27] Ercolano G, Harrington S A, Wang H, Tsai C F and MacManus-Driscoll J L 2010 *Supercond. Sci. Technol.* **23** 022003

[28] Gurevich A 2007 *Supercond. Sci. Technol.* **20** S128

[29] Brandt E H 1992 *Phys. Rev. Lett.* **69** 1105

[30] Koshelev A E and Kolton A B 2011 *Phys. Rev. B* **84** 104528

[31] Mele P, Guzman R, Gazquez J, Puig T, Obradors X, Saini S, Yoshida Y, Mukaida M, Ichinose A, Matsumoto K and Adam M I 2015 *Supercond. Sci. Technol.* **28** 024002

[32] Paulius L M, Fendrich J A, Kwok W K, Koshelev A E, Vinokur V M, Crabtree G W, and Glagola B G 1997 *Phys. Rev. B.* **56** 913
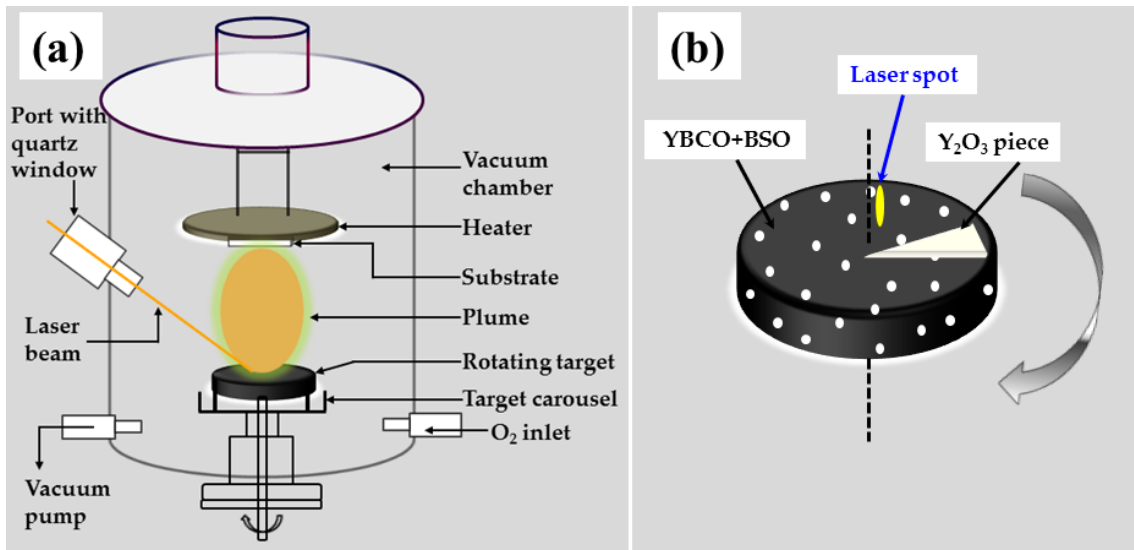
Figure captions:

Fig. 1: Schematic diagram of (a) the PLD chamber and (b) used targets for the deposition of YBCO films with artificial pinning centers..
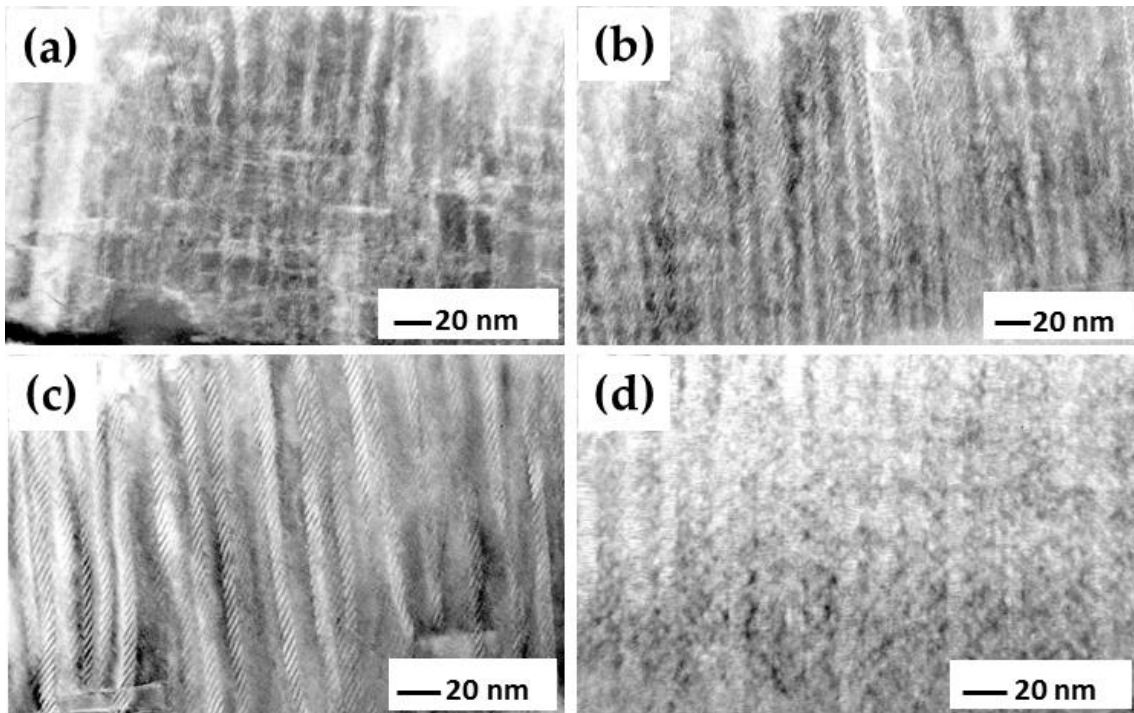
Fig. 2: The actual microstructure (cross-sectional view) of (a) YBCO+BSO2% (b) YBCO+BSO2%+YOB (c) YBCO+BSO4% and (d) YBCO+BSO4%+YOB nanocomposite films as observed by transmission electron microscope.

Fig. 3: High resolution TEM image (cross-sectional view) of (a) YBCO+BSO2%+YOA and (b) YBCO+BSO4%+YOA nanocomposite films. The inset shows the planar view of the TEM images of respective thin films.

Fig. 4: Variation of irreversibility field with temperature for (a) YBCO+BSO2% series (b) YBCO+BSO3% series (c) YBCO+BSO4% series and (d) all samples together.

Fig. 5: Variation of critical current density (J_C) and pinning force density (F_p) with respect to applied magnetic field for YBCO films with varying concentrations of APCs at 77 K (a), (b) and at 65 K (c), (d). The in-field J_C enhancement can be clearly observed for YBCO films with APCs. Systematic increase of $F_{pmax.}$ with respect to the APC concentration in the YBCO films can also be seen.

Fig. 6: Variation of $F_{pmax.}$ and $B_{max.}$ with respect to Y_2O_3 content for YBCO films with hybrid APCs at: 77 K (a), (b) and 65 K (c), (d).

Fig. 7: Comparison of angular dependence of J_C at 77 K, 1 T for (a) YBCO+BSO2% series (b) YBCO+BSO3% series (c) YBCO+BSO4% series and (d) all samples together. The enhancement in J_C along the entire angular regime can be observed for YBCO films with varying concentration of hybrid APCs.

Fig. 8: Comparison of angular dependence of J_C at 65 K, 3 T for (a) YBCO+BSO2%

series (b) YBCO+BSO3% (c) YBCO+BSO4% and (d) all samples together. The enhancement in J_C along the entire angular regime can be observed for YBCO films with varying concentration of hybrid APCs.

Fig. 9: Schematic diagram of (a) vortex configuration at different inclination of applied magnetic field with respect to the c-axis of the samples and (b) pinning of vortices provided by YO nanoparticles distributed randomly in the YBCO matrix.

Table captions:

Table 1: Structural parameters for the superconducting samples as obtained from the XRD measurements

List of Figures

Fig. 1: Schematic illustration of (a) the PLD chamber and (b) used targets for the deposition of YBCO films with artificial pinning centers.

Fig. 2: The actual microstructure (cross-sectional view) of (a) YBCO+BSO2% (b) YBCO+BSO+YOB (c) YBCO+BSO4% and (d) YBCO+BSO4%+YOB nanocomposite as observed by transmission electron microscope.
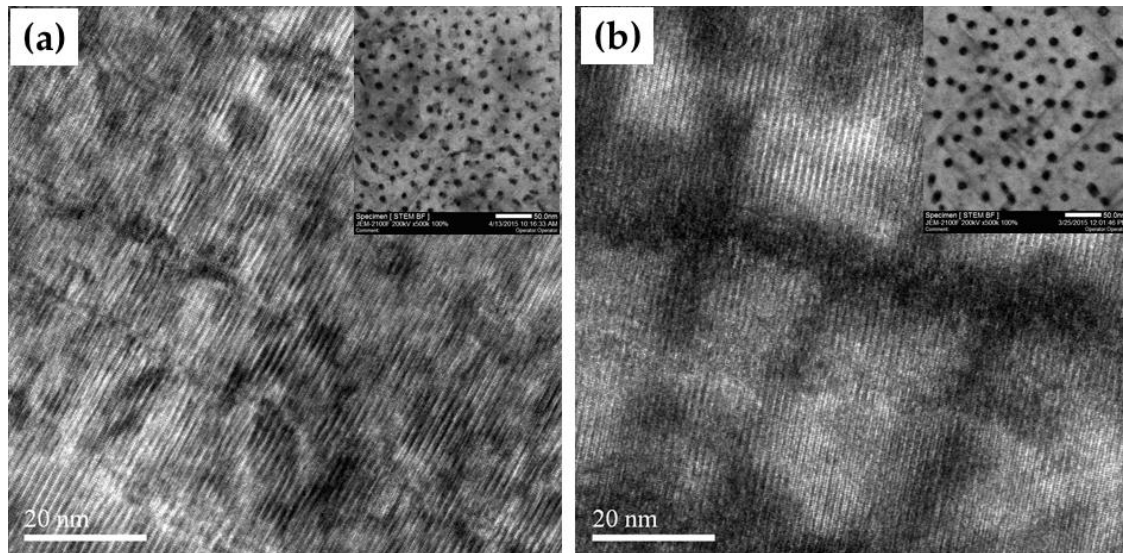

Fig. 3: High resolution TEM image (cross-sectional view) of (a) YBCO+BSO2%+YOA and (b) YBCO+BSO4%+YOA nanocomposite films. The inset shows the planar view of the TEM images of respective thin films.
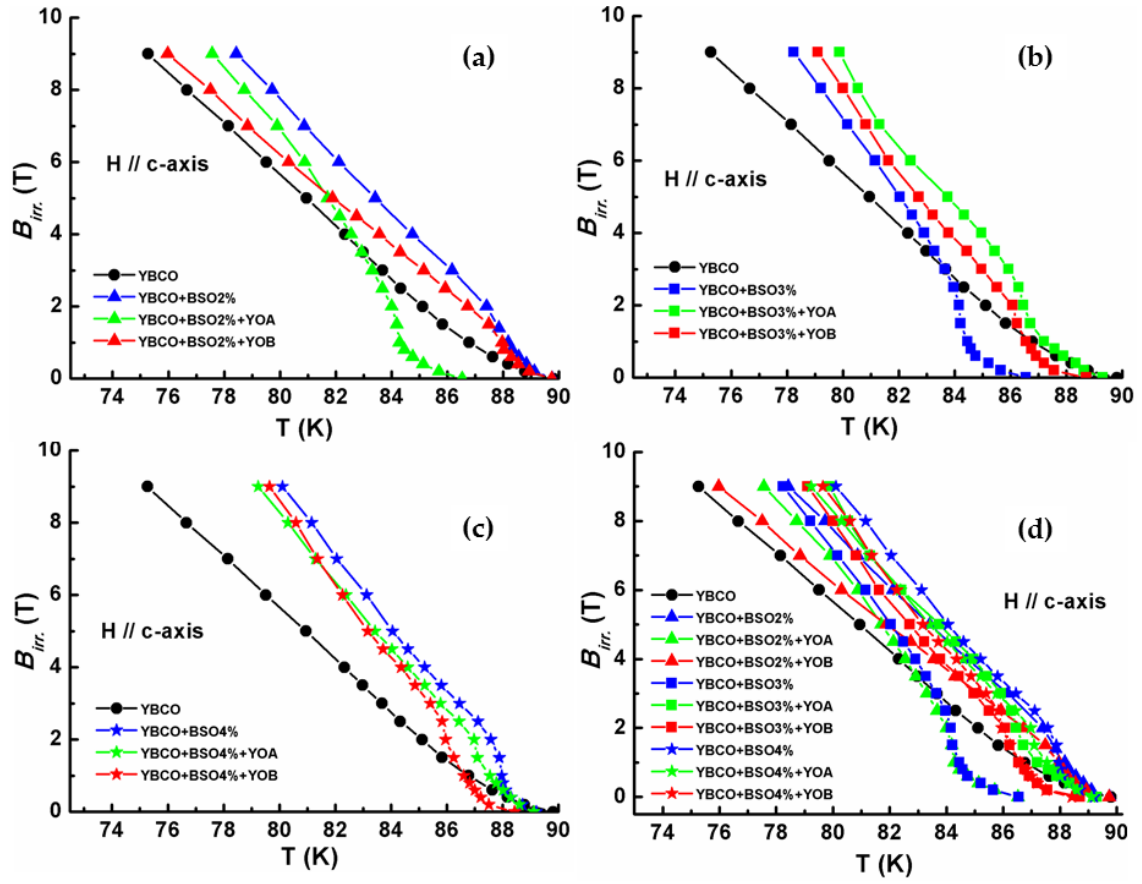
Fig. 4: Variation of irreversibility field with temperature for (a) YBCO+BSO2% series (b) YBCO+BSO3% series (c) YBCO+BSO4% series and (d) all samples together.
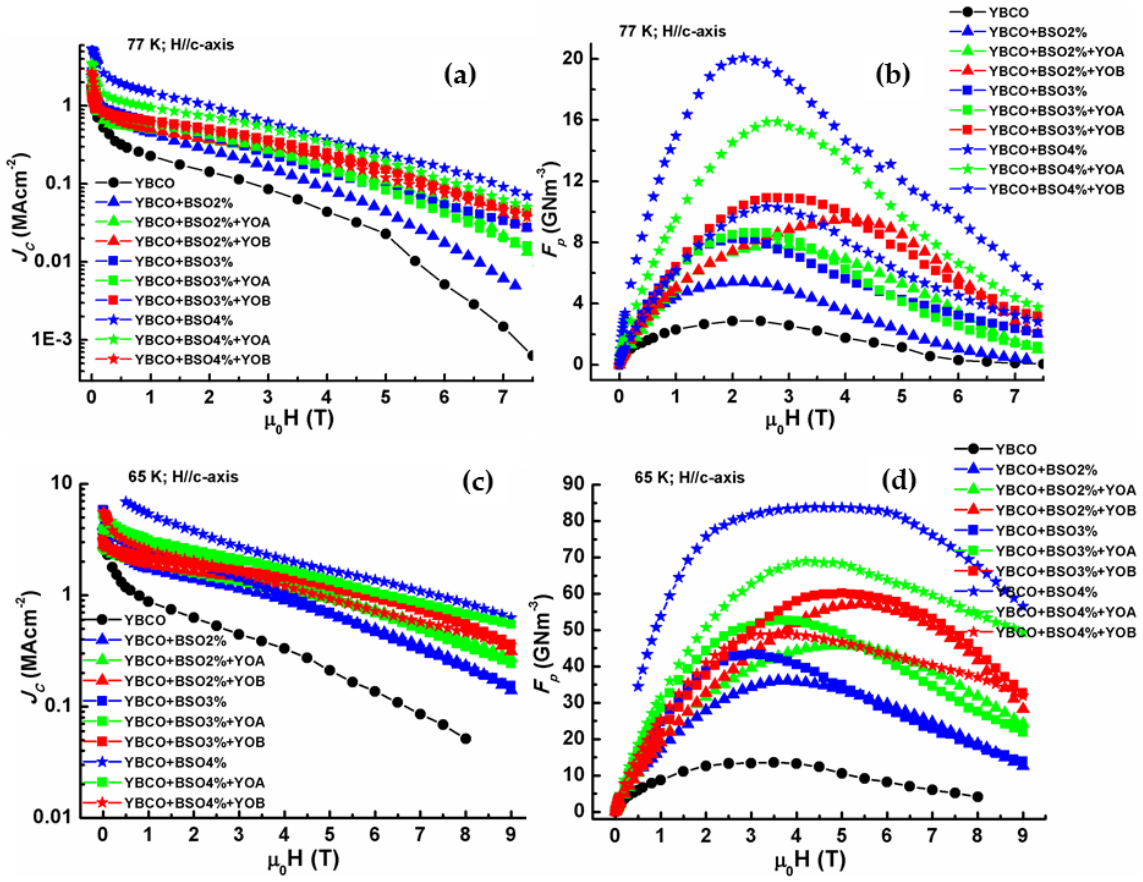
Fig. 5: Variation of critical current density (J_C) with respect to applied magnetic field for YBCO films with varying concentrations of APCs at 77 K for (a) YBCO+BSO2% series (b) YBCO+BSO3% series (c) YBCO+BSO4% series and (d) all samples together. The in-field J_C enhancement can be clearly observed for YBCO films with APCs.
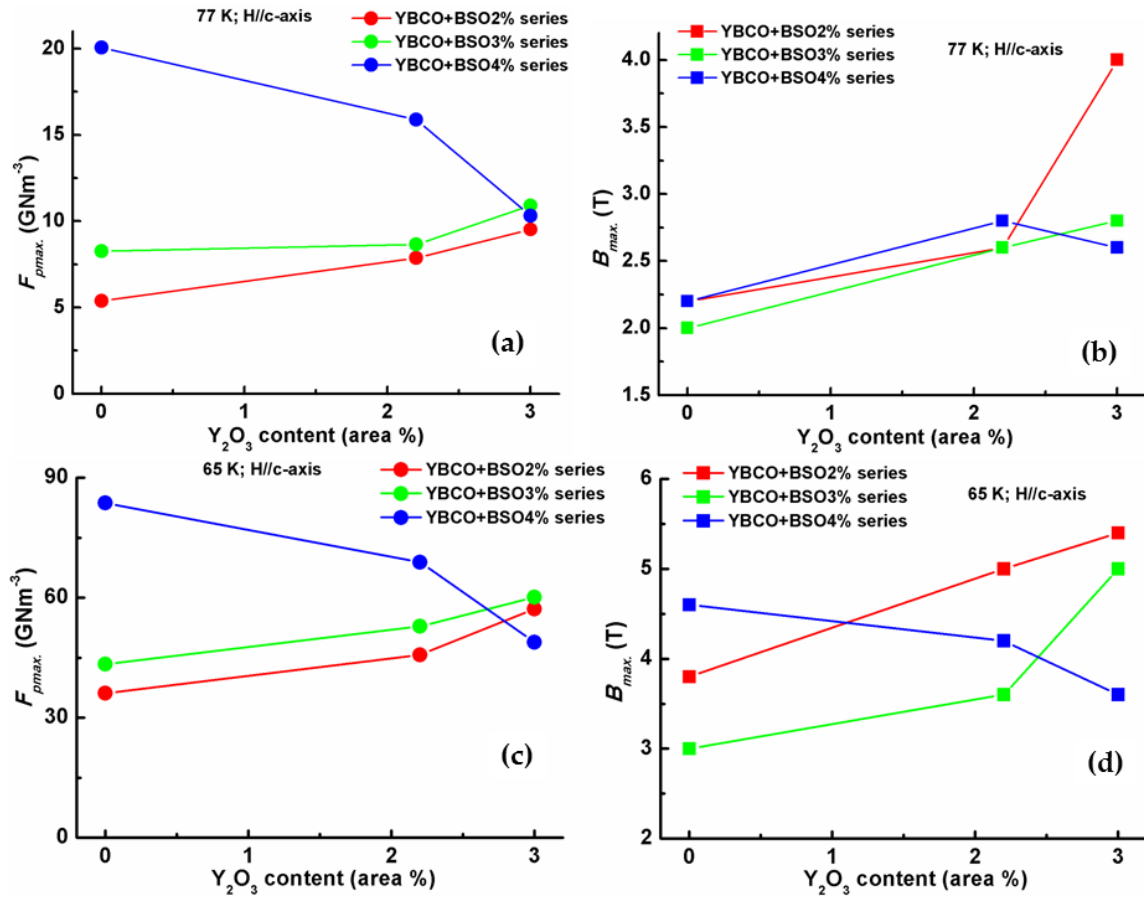
Fig. 6: Variation of $F_{pmax.}$ and $B_{max.}$ with respect to Y_2O_3 content for YBCO films with hybrid APCs at: 77 K (a), (b) and 65 K (c), (d).
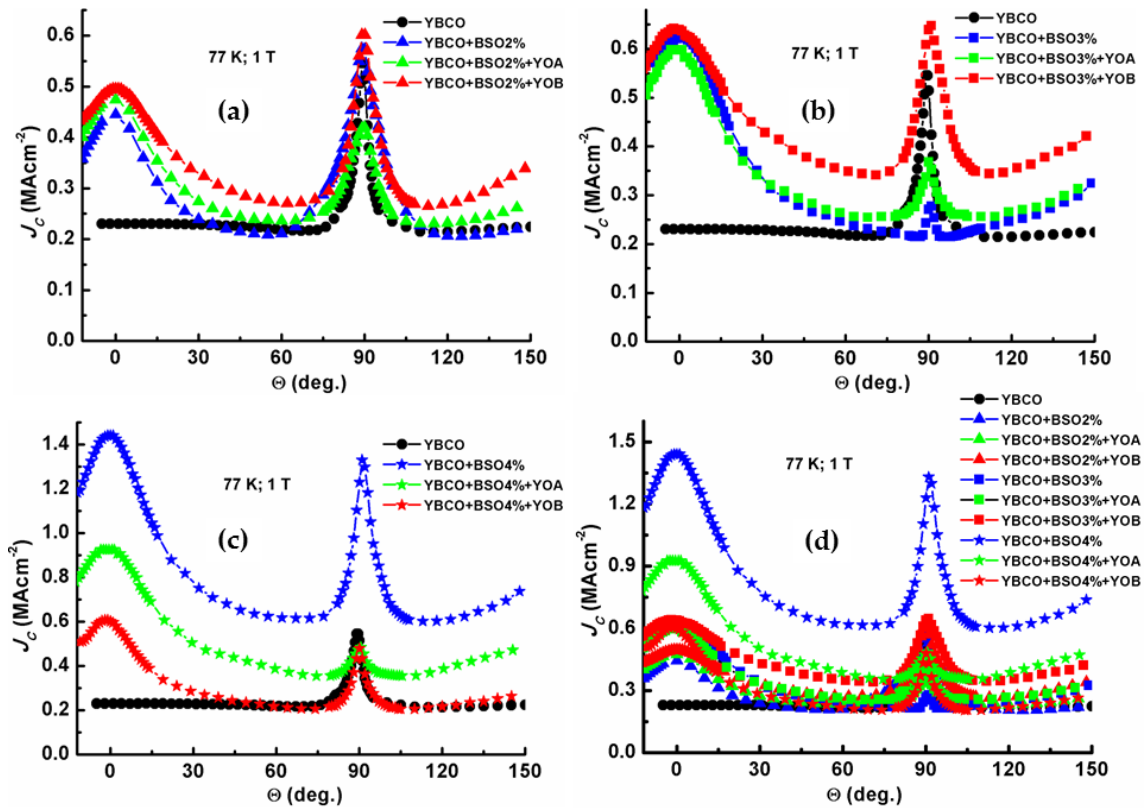
Fig. 7: Comparison of angular dependence of J_C at 77 K, 1 T for (a) YBCO+BSO2% series (b) YBCO+BSO3% (c) YBCO+BSO4% and (d) all samples together. The enhancement in the value along the entire angular regime can be observed for YBCO films with varying concentration of hybrid APCs.
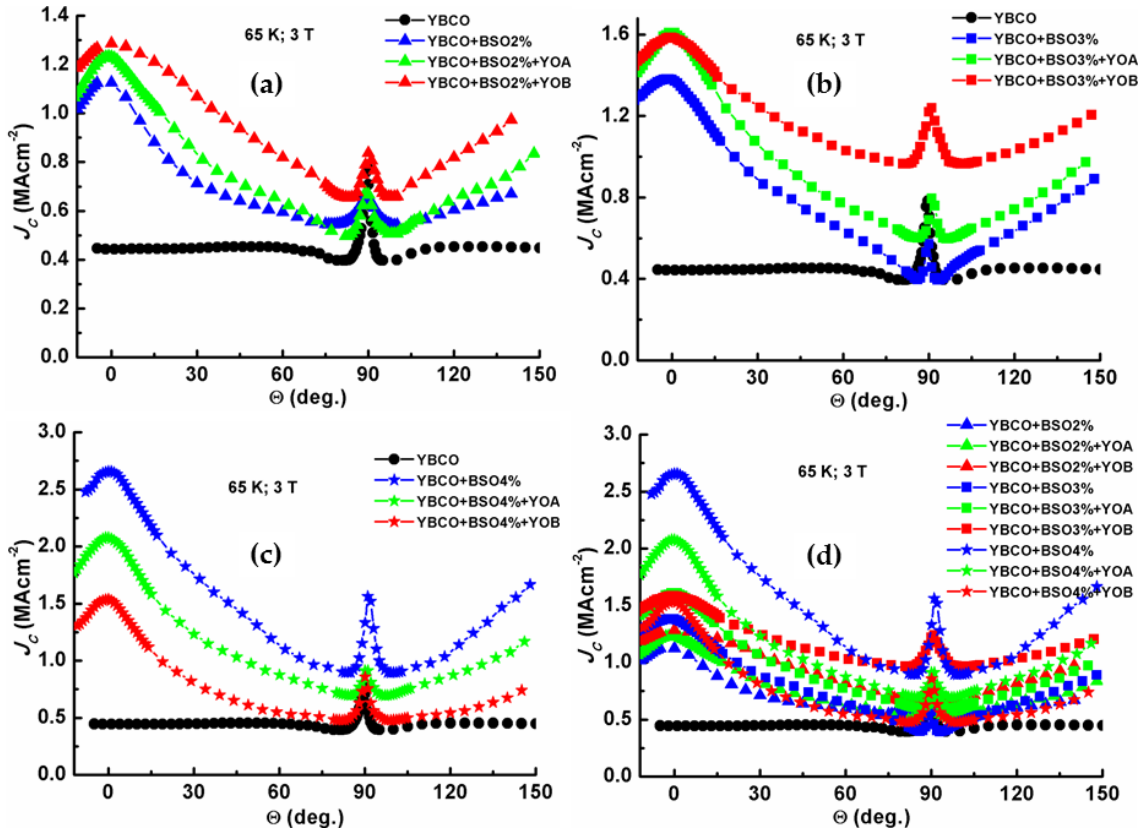
Fig. 8: Comparison of angular dependence of J_C at 65 K, 3 T for (a) YBCO+BSO2% series (b) YBCO+BSO3% (c) YBCO+BSO4% and (d) all samples together. The enhancement in the value along the entire angular regime can be observed for YBCO films with varying concentration of hybrid APCs.
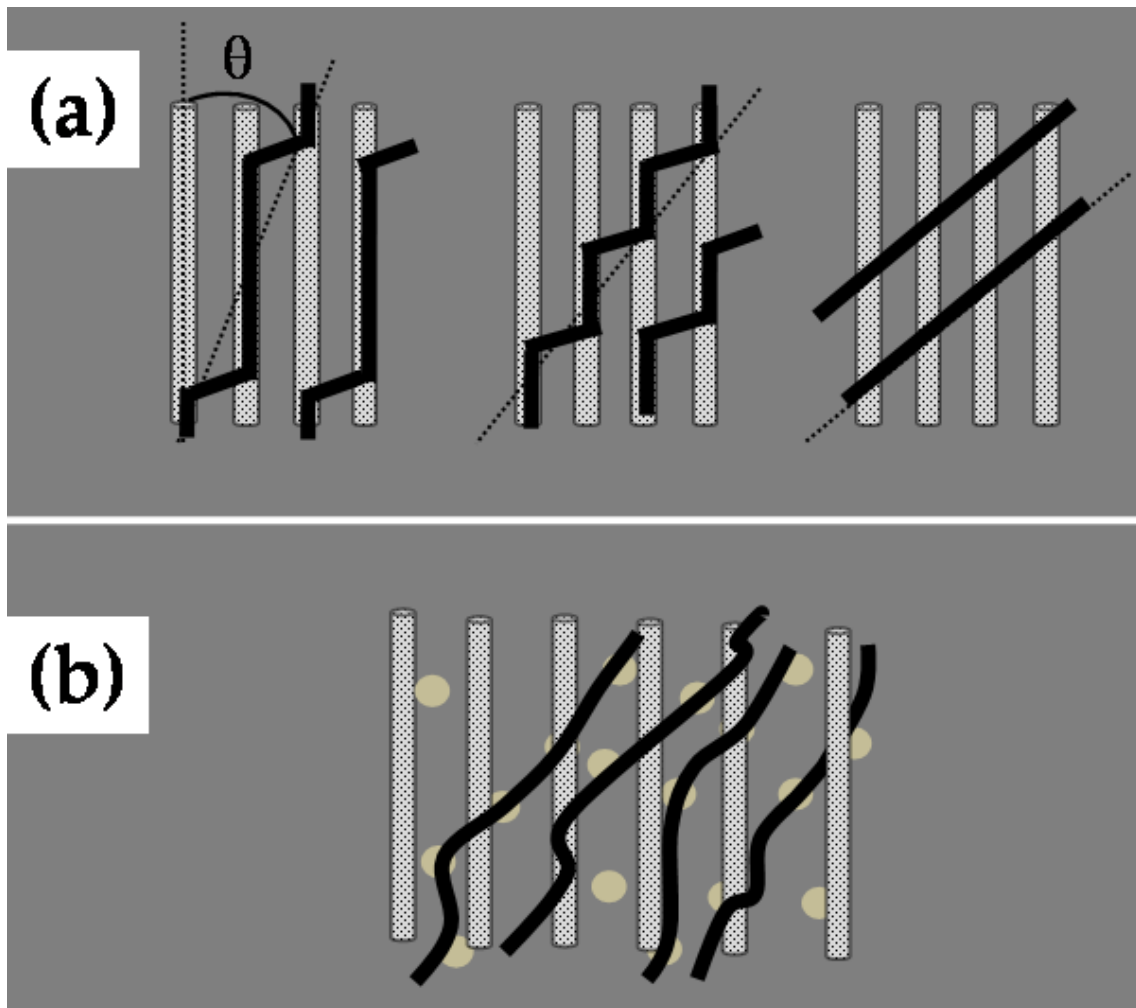
Fig. 9: Schematic diagram of (a) vortex configuration at different inclination of applied magnetic field with respect to the c-axis of the samples and (b) pinning of vortices provided by YO nanoparticles distributed randomly in the YBCO matrix.

List of Tables

Table 1: Structural parameters for the superconducting samples as obtained from the XRD measurements

COMPOSITION		c-axis (Å)	$\Delta\omega$ (005) (deg.)	$\Delta\phi$ (103) (deg.)
YBCO		11.687	0.26	1.05
YBCO+BSO2%	No Y_2O_3	11.718	0.22	1.1
	Y_2O_3 A	11.743	0.46	1.20
	Y_2O_3 B	11.747	0.26	1.12
YBCO+BSO3%	No Y_2O_3	11.704	0.20	0.68
	Y_2O_3 A	11.712	0.14	0.80
	Y_2O_3 B	11.76	0.27	1.31
YBCO+BSO4%	No Y_2O_3	11.694	0.19	1.21
	Y_2O_3 A	11.704	0.17	1.15
	Y_2O_3 B	11.708	0.17	1.38